Primitive Chain Network Simulations for Comb-Branched Polymer under Step Shear Deformations

Yuichi Masubuchi*, Yumi Matsumiya, Hiroshi Watanabe

Institute for Chemical Research, Kyoto University,

Gokasyo, Uji, Kyoto, 611-0011 Japan

Seiji Shiromoto, Masaaki Tsutsubuchi and Yoshiaki Togawa

Sumitomo Chemical Co., Ltd.

2-1, Kitasode, Sodegaura City, Chiba 299-0295, Japan

*Correspondence should be addressed

e-mail: mas@scl.kyoto-u.ac.jp

submitted to Rheo. Acta. on Apr. 26 2011

revised by YM, June 15 2011

Abstract

The damping of the relaxation modulus under step shear deformation is weaker for multi-branched polymers such as comb polymers than for linear polymers. This weak damping has been related to the hierarchical relaxation, the branched arm relaxation occurring prior to the backbone relaxation and dilating the entanglement network for the backbone relaxation/contraction. A corresponding model has been proposed and favorably compared with the data for the damping function. However, the enhancement of dilation due to large deformation, known to occur for linear polymers to affect the chain contraction rate, was not considered in the model. Thus, in this paper, we investigated the dilation for a comb polymer under deformation with the aid of a 3D multichain sliplink simulation that naturally accounts for the dilation due to the constraint release through the many chain dynamics. The simulation was confirmed, to the first time, to reproduce the linear and nonlinear viscoelastic data for a comb polyisoprene [Kirkwood et al Macromolecules 2009]. A magnitude of dilation under deformation was examined for the survival probability of the sliplinks. It turned out that the dilation for the comb backbone activated by the arm relaxation is enhanced by the deformation at short times but *not* at long times where the backbone relaxes and the damping function is defined. This result lends support to the conventional model.

Introduction

Entangled polymers exhibit significant nonlinearity in their viscoelastic relaxation under large deformation, and this nonlinearity is intimately related to the processability (Tadmor and Gogos 2006). According to the K-BKZ constitutive equation (Bernstein et al. 1963), the characteristic measure of the nonlinearity is the damping function that describes the non-linear decrease of the relaxation modulus under large deformation. In particular, multi-branch polymers such as combs and branch-on-branch dendrimers are known to exhibit weaker damping compared to linear and star-branched polymers (Laun 1978, Osaki 1993). This weak damping of multi-branch polymers has been related to the hierarchical relaxation, the branched arm relaxation occurring prior to the backbone relaxation and dilating the entanglement network for the backbone relaxation (McLeish 1988). Specifically, Vega and Milner (2007) focused on a reduction of the effective entanglement density for the backbone: Since the branched arm relaxes faster than the backbone, the multi-branch polymer effectively behaves as a linear polymer in solution (with the relaxed arm serving as the solvent) in a long time scale where the damping function is defined. If the backbone volume fraction is relatively small, the backbone has scarce entanglements thereby showing the weak damping analogous to that observed for low molecular weight linear polymers (Osaki 1993, Osaki et al 1998).

Kapnistos et al (2009) have semi-quantitatively examined the hierarchical relaxation

picture with the slip-spring model (Likhtman 2005). In their model, a Rouse chain is constrained by a set of discrete virtual springs each of which is anchored in space at one end and attached, at the other end, to the chain through a sliplink. Thus, the density of the topological constraint can be tuned with the number n_{vs} of the virtual springs per chain. Indeed, Kapnistos et al (2009) have reported that the magnitude of nonlinear damping lies between those for the Rouse model (no damping) and the Doi-Edwards model (Doi and Edwards 1986) if n_{vs} is small. Although they have not made any simulation for branch polymers, they focused on the semi-quantitative agreement of their simulation for linear polymers with small n_{vs} and experiments for comb polymers to rationalize the hierarchical relaxation of comb polymers.

Kirkwood et al (2009) have further developed the hierarchical relaxation picture and proposed a theoretical description of the damping function of multi-branch polymer. In the time scale for the backbone relaxation, the tube diameter a increases due to the dilation activated by the relaxation of the arms and the backbone ends as $a = a_0\phi_{BB}^{-1/2}$ where a_0 is the original tube diameter and ϕ_{BB} is the volume fraction of the unrelaxed portion of the backbone. This increase of tube diameter reduces the primitive path length L measured along the dilated tube axis as $L = Z^0_{bb}a_0\,\phi_{BB}^{1/2}$ where Z^0_{bb} is number of entanglement segment along the backbone. This relaxation of the primitive path length occurs even under deformation and therefore the primitive path length after the arm relaxation is expressed as $L = \lambda(\gamma)\,\phi_{BB}^{1/2}\,Z^0_{bb}a_0$ where $\lambda(\gamma)$ is the chain stretch at the

deformation. Thus the effective stretch of the backbone from its original length is obtained as L / $Z^0_{bb}a_0 = \lambda(\gamma)\,\phi_{BB}^{1/2}$ and the corresponding effective strain is written as $\gamma\phi_{BB}^{1/2}$. Substituting this effective strain into the approximated Doi-Edwards damping function, they obtained the damping function as a function of ϕ_{BB} as $h(\gamma, \phi_{BB}) = 1/ (1+ 4\phi_{BB}\gamma^2/15)$. The obtained damping function was in reasonable agreement with experiments.

In spite of the abovementioned success of the hierarchical picture, it has been pointed out that the effect of deformation on the dilation was not considered in the above treatment, e.g., it is assumed that ϕ_{BB} does not depend on strain. According to the Doi-Edwards theory (Doi and Edwards 1986), the chain contraction under the deformation results in a loss of the constraints, and the damping is indeed explained in terms of the magnitude of this loss. The loss of constraint would be negligible for the backbone unless the branch point withdrawal takes place (Archer and Varshney 1998). On the other hand, for the branched arm, the deformation may enhance the dilation compared to that at equilibrium.

Thus, in this study, we examined the dilation process of comb polymer under deformation by using 3D multi-chain sliplink simulation called primitive chain network simulation (Masubuchi et al. 2001). This was the first attempt of the quantitative simulation for the comb polymer (although the simulations had been conducted earlier for multi-branch (H-shaped) polymer (Masubuchi et al 2006) and star polymers (Masubuchi et al 2004, 2011).) For both linear and

nonlinear relaxation, the simulation results were found to be in reasonable agreement with the experimental data for comb polymer melt (Kirkwood et al. 2009). The dilation of the entanglement network under step deformation, the main target of this study, was quantified through the survival probability of the sliplinks. The extra dilation due to the deformation was indeed observed at short times (where the arms relaxed) but *not* at long times where the backbone relaxed and its damping function was defined, which lends support to the model of hierarchical relaxation under the deformation (Kirkwood et al. 2009). Details of these results are presented in this paper.

Model and simulation

The simulation code utilized in this study, including a topological change around branch point, has been proposed earlier (Masubuchi et al. 2006, 2011). The polymer is represented by consecutive segments, sliplinks and branch point. Molar mass of the segment is assumed to be comparable to the entanglement molecular weight. The sliplink bundles segments in pair to form a network in 3D space. The polymer motion is described by Langevin-type equations for the spatial displacement of sliplinks, chain ends, and branch points, and for a change of the monomer number in each segment due to the monomer transport through the sliplink. The equations incorporate the chain elasticity, the chemical potential gradient, the friction against the medium, and the Brownian

random force. In addition to the branch point motion and the chain sliding, a topological change of the network was activated through creation and destruction of the sliplinks at the chain ends to represent hooking and unhooking among the chains. For multi-branch polymers, a further topological change is activated around the branch point to realize the curvilinear hopping of the branch point along the backbone (McLeish 1988). When all sliplinks on an arm disappear simultaneously, the hopping is achieved by a jump of the branch point to the next segment across the neighboring sliplink following the algorism proposed earlier (Shanbhag and Larson 2004). We assume equal probability (1/3) for the choices among three events, the jumps toward two backbone directions and no jump. The last choice (no jump) is incorporated to represent an event that the retracted arm does not penetrate into the next sliplink but hooks another surrounding chain.

In the actual simulation runs, the average equilibrium length of the segment, a (the undilated network mesh size), was chosen as the unit length, kT as the unit energy, $\tau_0=\zeta a^2/6kT$ with ζ = friction coefficient of the sliplink as the unit time. For comparison with the experimental data, we utilized the unit of molecular weight M_0 (and the corresponding unit stress G_0) as a fitting parameter rather than the molecular weight calculated from the unit length a. For the calculation of linear viscoelasticity, simulations under quiescent condition were performed for sufficient long time (10 times longer than the longest relaxation time, at least) to obtain linear relaxation modulus $G(t)$ as the auto-correlation function of shear stress. The auto-correlation function was calculated by the

fast multi-tau correlator algorism (Magatti and Ferri 2001) and converted into $G^*(\omega)$ by the REPTATE software (Ramirez and Likhtman 2009). The periodic boundary condition was employed with the simulation cell box of 8^3. For the relaxation modulus under step shear deformation, Lees-Edwards (Lees and Edwards 1972) shear boundary was used with the simulation cell of 16^3 for noise reduction. (It was confirmed that the results were essentially insensitive to the cell dimension in the range from 8^3 to 20^3 for the examined comb molecule for which the radius of gyration under equilibrium is ca. 4). In the simulation cell the deformation was applied affinely. The segment density was fixed at $10/a^3$ for both cases.

Results

Figure 1 compares the simulated linear viscoelastic G^* (= $G' + iG''$) with the data for a comb polyisoprene (Kirkwood et al. 2009) having the arm and backbone molecular weights of 10.2k and 85.1k, respectively, and 4.6 arms per backbone. In the simulation, the number of the segments was chosen to be 3, 5 and 3 for the arm, the backbone sequence between branch points, the end sequences of the backbone, respectively, and the arm number per backbone was set at 5. (These numbers were based on the unit molecular weight M_0=3.5k (Masubuchi et al. 2008) determined for linear polyisoprene melt (Matsumiya et al. 2000).) The other parameters for the fitting were $\tau_0 = 2.4$ sec and $G_0 = 0.49$ Pa; these values were determined from the data for linear

polymer after a correction of temperatures (40C^{o} for Matsumiya et al (2000) and -30C^{o} in Fig. 1) through the WLF shift reported by Kirkwood et al (2009). Note that here we neglect the difference in microstructure of the polyisoprene samples (Matsumiya et al. 2000 and Kirkwood et al. 2009) and thus further assessment on the parameters is required. Nevertheless as noted in Fig.1, the simulated G^* agrees reasonably well with the data. However, the arm and backbone relaxation processes seen at high and low frequencies have rather narrow mode distribution in the simulation compared to the data. A similar result was noted for the hierarchical relaxation model (Kirkwood et al. 2009), and the difference between the simulation and data can be due to a distribution in the branching structure/molecular weight of the comb sample. (For example, the slow terminal relaxation seen for the experimental G' data can be attributed to the slow component in the sample.)

Figure 2 compares the simulated relaxation modulus $G(t,\gamma)$ under large deformation with the data at 30˚C. The simulation parameters are $M_0 = 3.5$k, $\tau_0 = 1.0 \times 10^{-4}$ sec and $G_0 = 0.61$ MPa, being evaluated from the parameters utilized in Fig 1 after the WLF correction of temperature (30C^{o} in Fig.2). The simulation did not consider the glassy relaxation of the sample and thus underestimated $G(t,\gamma)$ at short times, $t < 10^{-3}$ sec. At longer t up to 10^{-1} sec, the simulation reproduces the data considerably well within the stress fluctuation in the simulation indicated in the small window in Figure 2. (The deviation seen at even longer $t > 10^{-1}$ sec can be again attributed to the a distribution in the branching structure/molecular weight of the comb sample.)

The time-strain separability of the simulated $G(t,\gamma)$ (Fig. 2) is examined in the top panel of Fig.3. It has been reported that due to the failure of the decoupling between chain stretch and orientation the time-strain separability is not valid under rigorous assessment but it is realized approximately in the margin of error (Sanchez-Reyes and Archer 2002 and Furuichi et al 2010). In this study the fluctuation of stress is not sufficiently small for the assessment of the separability (as shown in the small window in Fig.2). Thus we assumed the separability at long t, and the damping function $h(\gamma)$ was evaluated accordingly. Nevertheless for the smoothed data the separability is reasonably confirmed as shown in the top panel. In addition, as shown in the bottom panel, the $h(\gamma)$ thus obtained from the simulation (filled circles) is close to the data (unfilled circles; Kirkwood et al (2009)). The simulated $h(\gamma)$ and the data commonly exhibit the γ dependence weaker than the Doi-Edwards prediction (dashed curve).

Discussion

As judged from the agreement between the simulation and data seen in Figs. 1-3, the quality of the simulation appears to be satisfactorily high to give information for the dilation for the comb backbone under deformation. Specifically, we utilize the survival probability of the sliplinks, $\varphi(t)$, to represent the dilated entanglement mesh size as $a'(t) = a\ \varphi(t)^{-1/2}$ (with a = undilated mesh size) (Masubuchi et al. 2011). The top, middle, and bottom panels in the left column of Fig.4

show the time evolution of $\varphi(t,\gamma)$ under deformation defined for the comb molecule as a whole, the arm, and the backbone, respectively. As a reference for comparison, $\varphi(t,\gamma)$ simulated for a linear polymer (having 20 entanglements per chain) and a star polymer (with 4 arms each having 10 entanglements) is shown in the 3rd panels of Figures 5 and 6. The top panels of Figures 5 and 6 show the $G(t,\gamma)$ simulated for these linear and star chains. In Figures 4-6, the thick dashed curve indicates the quantities at equilibrium for $G(t,\gamma)$ and $\varphi(t,\gamma)$, and we refer these equilibrium quantities as $G(t)$ and $\varphi(t)$ hereafter.

We first focus on the behavior of the linear and star chains (Figures 5 and 6). The damping behavior of their relaxation modulus $G(t,\gamma)$ and the resulting damping function $h(\gamma)$ were in good agreement with experiments and thus $h(\gamma)$ was close to the Doi-Edwards prediction (Furuichi et al 2008, 2010). (Note that $G(t,\gamma)/G_0$ at $t/\tau_0=1$ is less than unity due to the fluctuation according to the force balance around sliplink as discussed earlier (Masubuchi et al 2003 and Furuichi et al 2008). This is consistent with the fact that our parameter G_0 is larger than the plateau modulus G_N.) The sliplink survival probability $\varphi(t,\gamma)$ of these chains under deformation (3rd panels) shows damping that reflects the extra unhooking induced by the chain contraction (Furuichi 2010). This damping is *qualitatively* similar to that seen for $G(t,\gamma)$. However, the damping is much weaker for $\varphi(t,\gamma)$ than for $G(t,\gamma)$ (compare 2nd and bottom panels showing the ratio $G(t,\gamma)/G(t)$ and $\varphi(t,\gamma)/\varphi(t)$), because $G(t,\gamma)$ is contributed from not only the dilation but also the chain orientation

and the chain stretch (Mead et al 1998). Another difference can be found for the time evolution of $G(t,\gamma)/G(t)$ and $\varphi(t,\gamma)/\varphi(t)$, that represent the time evolution of the nonlinearity. For both linear and star polymers, the $G(t,\gamma)/G(t)$ ratio is known to decrease monotonically with t and approaches the damping function $h(\gamma)$ at long t (Islam et al. 2001), as can be confirmed also from the presented behavior of $G(t,\gamma)/G(t)$. On the other hand, the $\varphi(t,\gamma)/\varphi(t)$ (bottom panels) first decreases and then increases with increasing t, as clearly shown for star polymer in Figure 6. This non-monotonic behavior of $\varphi(t,\gamma)$ is related to long-lived sliplinks that is formed between segments near the chain center and/or branch point. The curvilinear distance of such sliplinks measured from the chain/arm ends is large, so that the contraction of the chain/arm does not remove those sliplinks (and allows them to be long-lived). Those long-lived sliplinks tend to suppress the decay $\varphi(t,\gamma)$ at long t, which results in the non-monotonic change of the $\varphi(t,\gamma)/\varphi(t)$ ratio.

We should also note that the long-lived sliplinks hardly contribute to the modulus (or stress) since the long-lived sliplinks are rather scarce to constrain the orientational relaxation. For example, at $t/\tau_0 > 1000$ in Figures 5 and 6, $G(t,\gamma)$ has almost fully relaxed while $\varphi(t,\gamma)$ has not. At these t, each chain had less than one surviving sliplink and was subjected to no significant constraint against the orientational relaxation (stress relaxation).

Now, we turn our attention to the comb polymer (see Fig. 4). The above-mentioned feature of the $\varphi(t,\gamma)/\varphi(t)$ ratio is clearly noted for the arm (middle panel in the right column).

Namely, this ratio is the smallest and the damping is the strongest at intermediate times, $t \sim 10^{-2}$ sec. More importantly, $\varphi(t,\gamma)$ for the arm becomes insensitive to the deformation and approaches $\varphi(t)$ at equilibrium in a longer time scale of the backbone relaxation, $t > 10^{-1}$ sec. This feature suggests that the magnitude of dilation due to the arm relaxation is not affected by the deformation (and coincides with that at equilibrium) in the long time scale of the backbone relaxation. Consequently, $\varphi(t,\gamma)$ for the backbone (bottom panel) is not sensitive to the deformation and remains close to $\varphi(t)$ at equilibrium (thus ϕ_{BB} is virtually insensitive to γ). This result, indicating no extra deformation-induced dilation in the time scale of the backbone relaxation, lends support to the assumption made in the hierarchical models (Vega et al 2007, Kapnistos et al 2009, Kirkwood et al 2009).

In relation to our previous study (Furuichi et al 2010), we discuss the effect of convective constraint release (CCR). (Although the considered system is not under flow, we use the term CCR to express the mechanism that releases the entanglement on every occasion of the contraction of surrounding chains.) Figure 7 shows time evolution of sliplink number per molecule $N_s(t)$ normalized by its equilibrium value N_s^0. For linear and star polymers (top and middle panels), the ratio $N_s(t)/ N_s^0$ first decreases, shows a minimum at the characteristic time of chain contraction, and then increases for the longest relaxation time. The decrease of $N_s(t)/N_s^0$ is attributable to the CCR that is the removal of sliplinks for a given chain due to the chain contraction of surrounding chains.

Because the contraction becomes more significant under larger deformation, $N_s(t)/N_s^0$ decreases with an increase of strain. As we reported earlier (Furuichi et al 2010) this change of $N_s(t)/N_s^0$ induces the coupling between chain stretch and orientation, and consequently the rigorous time-strain separability is valid only at times comparable to the terminal relaxation time. Nevertheless, for the linear and star polymers CCR occurs considerably. On the other hand, for the comb polymer (bottom panel), the change of $N_s(t)/N_s^0$ occurs only in a short time region that corresponds to the arm relaxation ($t < 10^{-2}$ sec), and $N_s(t)/N_s^0$ is stable in time and insensitive to strain in the time scale of backbone relaxation ($t > 10^{-1}$ sec). That means CCR (disentanglement induced by chain contraction) does not significantly occur in the time scale of backbone relaxation. Thus the coupling between chain stretch and orientation induced by CCR is less significant for the comb polymer. This also lends support the hierarchical model (Vega et al 2007, Kapnistos et al 2009, Kirkwood et al 2009) where the effect of CCR is not considered.

Conclusions

Primitive chain network simulations were performed for comb polymer melt to investigate the dilation of entangled network under deformation. The simulation reproduced the linear ad nonlinear viscoelastic data of a model comb polyisoprene reasonably well. Analysis of the sliplink survival

probability $\varphi(t,\gamma)$ obtained from the simulation indicated that $\varphi(t,\gamma)$ for the arm approaches $\varphi(t)$ at equilibrium in the time scale of the backbone relaxation and $\varphi(t,\gamma)$ for the backbone reduces to $\varphi(t)$ at equilibrium accordingly. This result indicates that the deformation activates no significant extra dilation in that time scale, lending support to the conventional assumption in the hierarchical model for multi-branched polymers (Vega et al 2007, Kapnistos et al 2009, Kirkwood et al 2009). To discuss applicable range of the assumption for branch structure, magnitude of deformation, etc, further assessment is required for other experimental dataset and we are working on this direction.

It so appears that the primitive chain network simulation is capable to predict the nonlinear stress damping of multi-branch polymers. However, it should be noted that the branch point withdrawal (McLeish and Larson, 1998) was not taken account in the current algorism for the topological change around branch point. It should be also noted that the possibility of reduction in monomeric friction for stretched chains (Ianniruberto et al, 2011) was not considered. For this reason, the current simulation is not applicable for elongational flows (Heinrich et al, 2002), for example. Implementation of the branch point withdrawal is an important subject of our future work, and the results will be reported elsewhere.

Acknowledgement

This study was supported by Grant-in-Aid for Scientific Research (B) No 20340111.

References

Archer LA, Varshney SK (1998) Synthesis and relaxation dynamics of multiarm polybutadiene melts. Macromolecules 31: 6348-6355

Bernstein B, Kearsley EA, Zapas LJ (1963) A STUDY OF STRESS RELAXATION WITH FINITE STRAIN. Transactions of the Society of Rheology 7: 391-410

Doi M, Edwards SF (1986) The theory of polymer dynamics. Clarendon, Oxford

Furuichi K, Nonomura C, Masubuchi Y, Watanabe H (2010) Chain contraction and nonlinear stress damping in primitive chain network simulations. Journal of Chemical Physics 133:174902

Furuichi K, Nonomura C, Masubuchi Y, Watanabe H, Ianniruberto G, Greco F, Marrucci G (2008) Entangled polymer orientation and stretch under large step shear deformations in primitive chain network simulations. Rheologica Acta 47: 591-599

Heinrich M, Pyckhout-Hintzen W, Allgaier J, Richter D, Straube E, Read DJ, McLeish TCB, Groves DJ, Blackwell RJ, Wiedenmann A (2002) Arm relaxation in deformed H-polymers in elongational flow by SANS. Macromolecules 35: 6650-6664

Ianniruberto G, Brasiello A, Marrucci G (2011), Friction Coefficient does not stay constant in nonlinear viscoelasticity, Proc. 7th Annual European Rheology Conference: 61

Islam MT, Sanchez-Reyes J, Archer LA (2001) Nonlinear rheology of highly entangled polymer liquids: Step shear damping function. Journal of Rheology 45: 61-82

Kapnistos M, Kirkwood KM, Ramirez J, Vlassopoulos D, Leal LG (2009) Nonlinear rheology of model comb polymers. Journal of Rheology 53: 1133-1153

Kirkwood KM, Leal LG, Vlassopoulos D, Driva P, Hadjichristidis N (2009) Stress Relaxation of Comb Polymers with Short Branches. Macromolecules 42: 9592-9608

Laun HM (1978) DESCRIPTION OF NONLINEAR SHEAR BEHAVIOR OF A LOW-DENSITY POLYETHYLENE MELT BY MEANS OF AN EXPERIMENTALLY DETERMINED STRAIN DEPENDENT MEMORY FUNCTION. Rheologica Acta 17: 1-15

Lees AW, Edwards SF (1972) The computer study of transport processes under extreme conditions. Journal of Physics C: Solid State Physics 5:1921-1929

Likhtman AE (2005) Single-chain slip-link model of entangled polymers: Simultaneous description of neutron spin-echo, rheology, and diffusion. Macromolecules 38: 6128-6139

Magatti D, Ferri F (2001) Fast multi-tau real-time software correlator for dynamic light scattering. Applied Optics 40: 4011-4021

Masubuchi Y, Takimoto JI, Koyama K, Ianniruberto G, Marrucci G, Greco F (2001) Brownian simulations of a network of reptating primitive chains. Journal of Chemical Physics 115:4387–4394

Masubuchi Y, Ianniruberto G, Greco F, Marrucci G (2003) Entanglement molecular weight and frequency response of sliplink networks. Journal of Chemical Physics 119:6925-6930

Masubuchi Y, Ianniruberto G, Greco F, Marrucci G (2004) Molecular simulations of the long-time behaviour of entangled polymeric liquids by the primitive chain network model. Modelling and Simulation in Materials Science and Engineering 12: S91-S100

Masubuchi Y, Ianniruberto G, Greco F, Marrucci G (2006) Primitive chain network simulations for branched polymers. Rheologica Acta 46: 297-303

Masubuchi Y, Lanniruberto G, Greco F, Marrucci G (2008) Quantitative comparison of primitive chain network simulations with literature data of linear viscoelasticity for polymer melts. Journal of Non-Newtonian Fluid Mechanics 149: 87-92

Masubuchi Y, Yaoita T, Matsumiya Y, Watanabe H (2011) Primitive chain network simulations for asymmetric star polymers Journal of Chemical Physics 134: 194905

Matsumiya Y, Watanabe H, Osaki K (2000) Comparison of Dielectric and Viscoelastic Relaxation Functions of cis-Polyisoprenes: Test of Tube Dilation Molecular Picture. Macromolecules 33: 499-506

McLeish TCB (1988) HIERARCHICAL-RELAXATION IN TUBE MODELS OF BRANCHED POLYMERS. Europhysics Letters 6: 511-516

McLeish TCB, Larson RG (1998) Molecular constitutive equations for a class of branched polymers: The pom-pom polymer. Journal of Rheology 42: 81-110

Mead DW, Larson RG, Doi M (1998) A Molecular Theory for Fast Flows of Entangled Polymers. Maccromolecules 31:7895-7914

Osaki K (1993) ON THE DAMPING FUNCTION OF SHEAR RELAXATION MODULUS FOR ENTANGLED POLYMERS. Rheologica Acta 32: 429-437

Osaki K, Takatori E, Shibasaki S, Kurata M (1988) STRESS-RELAXATION OF SEMIDILUTE POLYSTYRENE SOLUTIONS - A NEW OBSERVATION WITH THETA-SOLVENT AND WITH BLENDS CONTAINING VERY SHORT CHAINS. Polymer Journal 20: 511-513

Ramirez J, Likhtman AE (2009) http://reptate.com

Sanchez-Reyes J, Archer LA (2002), Step Shear Dynamics of Entangled Polymer Liquids, Macromolecules 35:5194-5202

Shanbhag S, Larson RG (2004) A slip link model of branch-point motion in entangled polymers Macromolecules 37: 8160-8166

Tadmor Z, Gogos CG (2006) Principles of Polymer Processing. Wiley, New Jersey.

Vega DA, Milner ST (2007) Shear damping function measurements for branched polymers. Journal of Polymer Science Part B-Polymer Physics 45: 3117-3136

Figure Captions

Figure 1 Storage modulus (G') and loss modulus (G'') of comb polyisoprene (PI132 in Kirkwood et al (2009)). Filled and unfilled circles indicate the G' and G'' data. Solid and dashed lines are from simulation.

Figure 2 Relaxation modulus of comb polyisoprene under step shear deformations. Symbols are the same as in Kirkwood et al (2009), and the initial strain is 0.5, 1.0, 2.0, 3.0, 4.0 and 5.0 from top to bottom. Solid curves are from simulation under the corresponding strain. Thick dashed curve is the simulated linear relaxation modulus. Small window shows the bare simulation data without smoothing.

Figure 3 Test of time-strain separability (top panel) and the resulting damping function (bottom panel) for the simulation data presented in Fig. 2. Thick curve in the top panel indicates the linear relaxation modulus. In the bottom panel, unfilled circles show the experimental data (Kirkwood et al. 2009), filled circles are from the simulation, and the dashed curve indicates the Doi-Edwards damping function.

Figure 4 Sliplink survival probability $\varphi(t,\gamma)$ (left panels) and the ratio $\varphi(t,\gamma)/\varphi(t)$ (right panels)

simulated for the whole molecule of the comb polymer (top panel), the arms (middle panel), and the backbone (bottom panel) during the stress relaxation process examined in Fig. 2. Solid curves and unfilled circles indicate the probability under step shear strains ranging from 0.5 to 5.0. Thick dashed curve for $\varphi(t,\gamma)$ indicates the probability $\varphi(t)$ at equilibrium.

Figure 5 Relaxation modulus $G(t,\gamma)$ (top panel) and sliplink survival probability $\varphi(t,\gamma)$ (3rd panel from the top) of a linear polymer (M=20M_0). The ratio $G(t,\gamma)/G(t)$ (2nd panel) and $\varphi(t,\gamma)/\varphi(t)$ (bottom panel) are also shown. Solid curves and unfilled circles indicate the behavior under step shear strains of 0.5, 1.0, 2.0, 3.0, 4.0 and 5.0. Thick dashed curves for $G(t,\gamma)$ and $\varphi(t,\gamma)$ show the behavior at equilibrium, $G(t)$ and $\varphi(t)$.

Figure 6 Relaxation modulus $G(t,\gamma)$ (top panel) and sliplink survival probability $\varphi(t,\gamma)$ (3rd panel from the top) of a 4-arm star polymer (M=40M_0, M_a=10M_0). The ratio $G(t,\gamma)/G(t)$ (2nd panel) and $\varphi(t,\gamma)/\varphi(t)$ (bottom panel) are also shown. Solid curves and unfilled circles indicate the behavior under step shear strains of 0.5, 1.0, 2.0, 3.0, 4.0 and 5.0. Thick dashed curves for $G(t,\gamma)$ and $\varphi(t,\gamma)$ show the behavior at equilibrium, $G(t)$ and $\varphi(t)$.

Figure 7 Sliplink number per molecule N_s(t) normalized by its equilibrium value N_s^0 under step

shear strains of 0.5, 1.0, 2.0, 3.0, 4.0 and 5.0 for linear (top), star (middle) and comb (bottom) polymers.

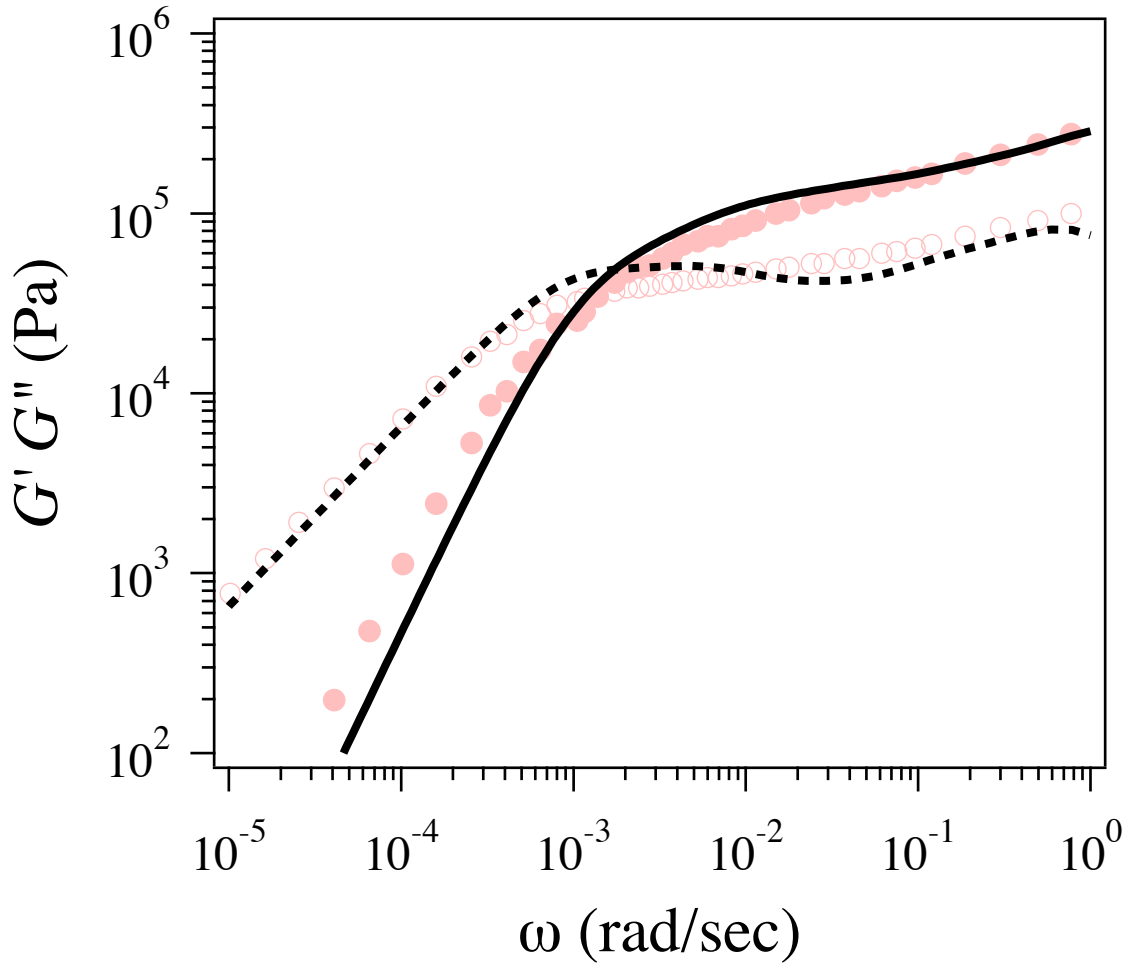

Figure 1 Masubuchi et al

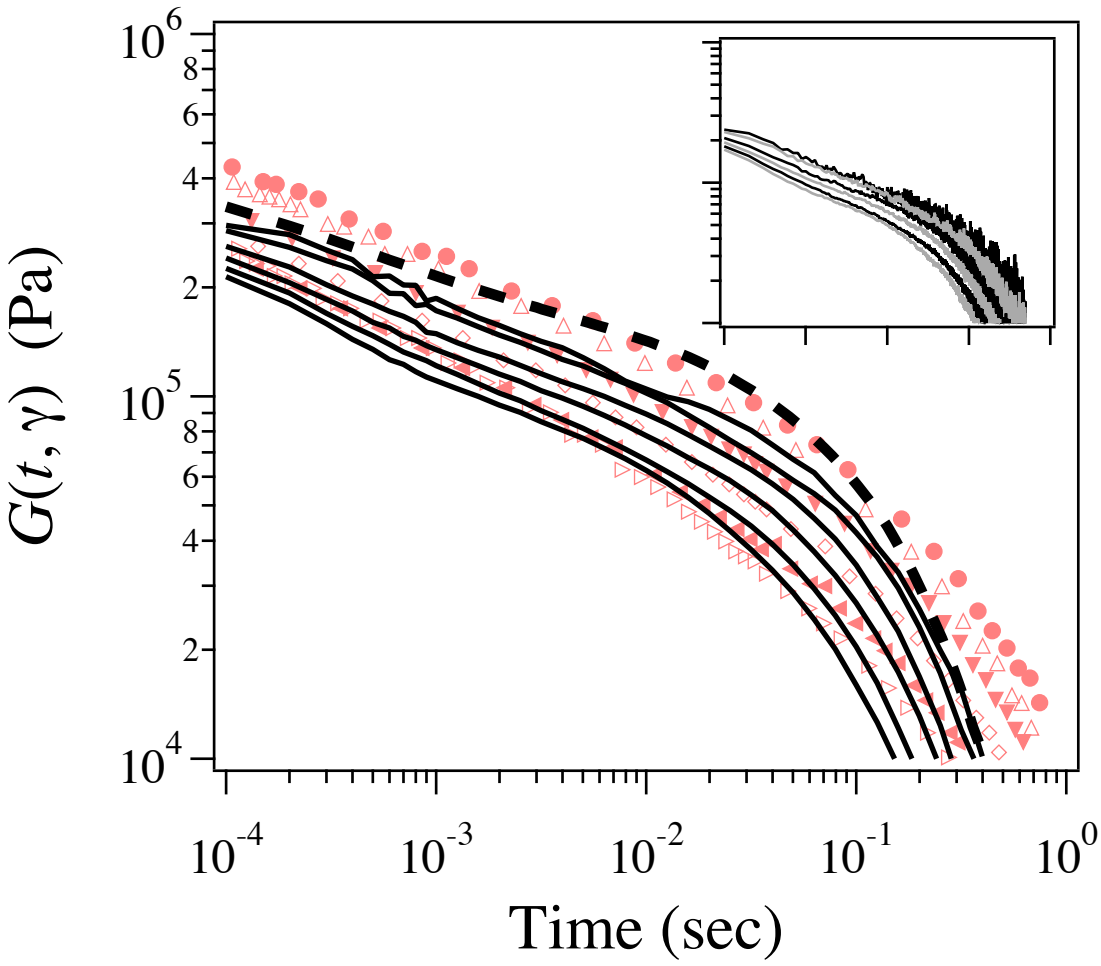

Figure 2 Masubuchi et al

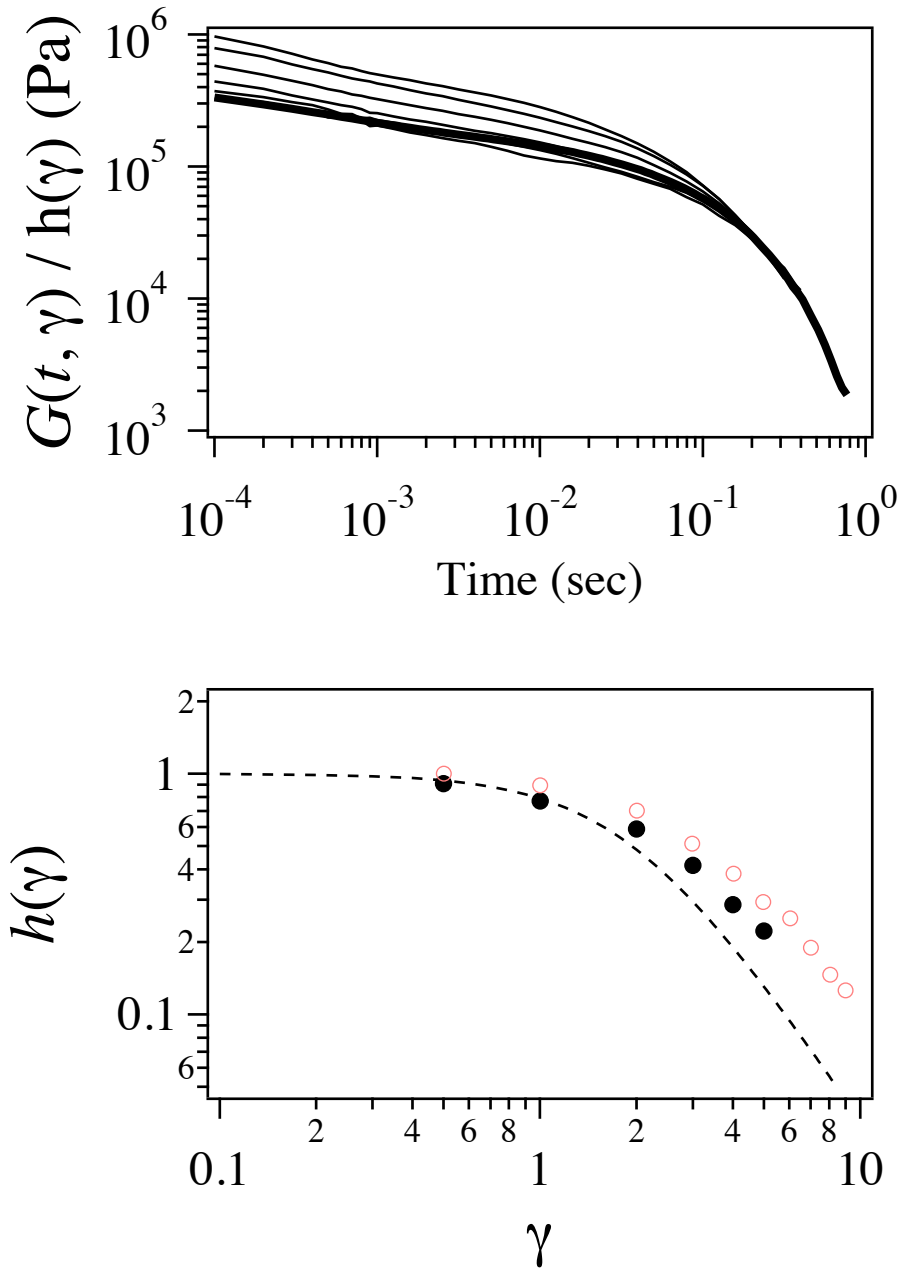

Figure 3 Masubuchi et al

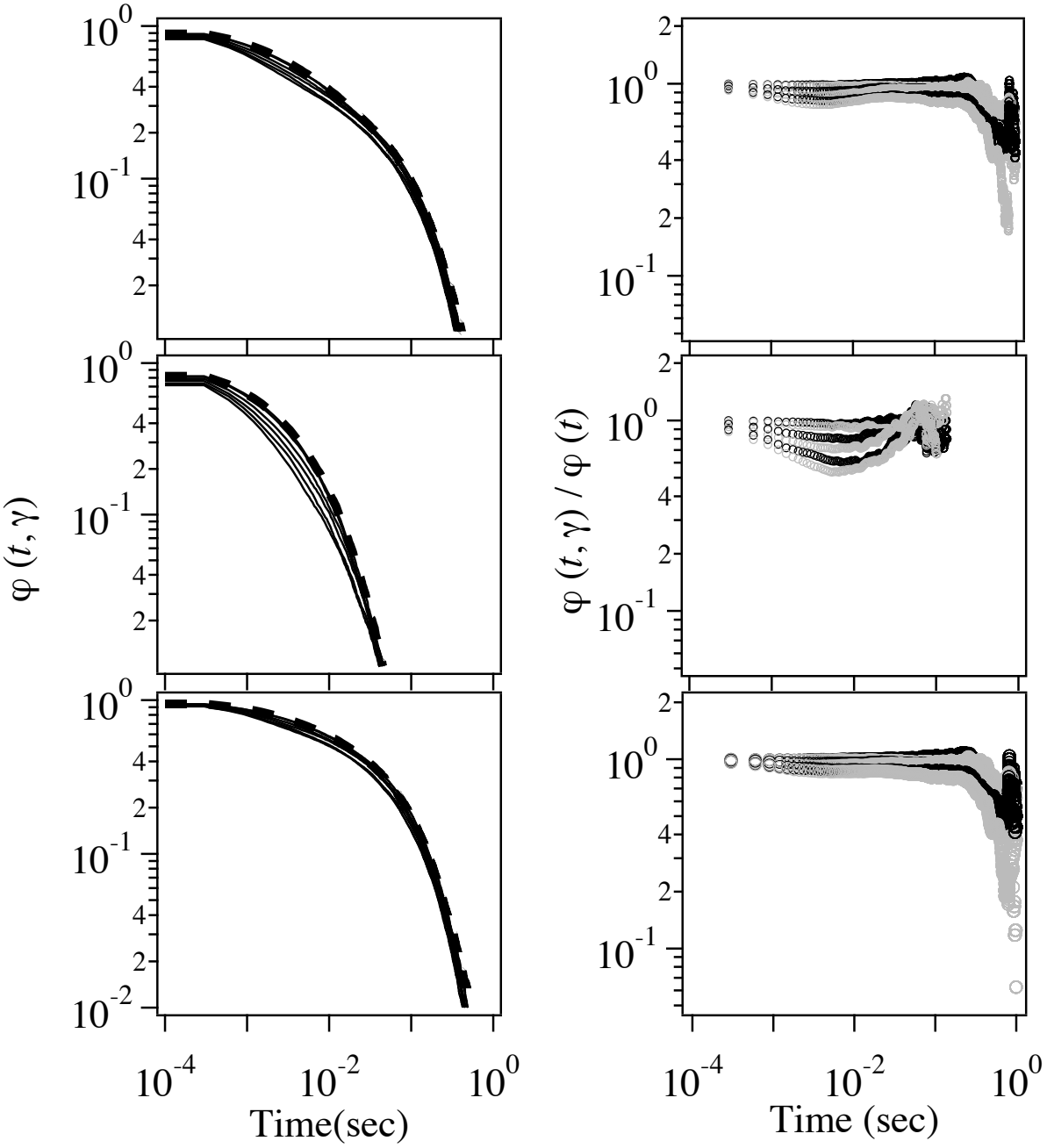

Figure 4 Masubuchi et al

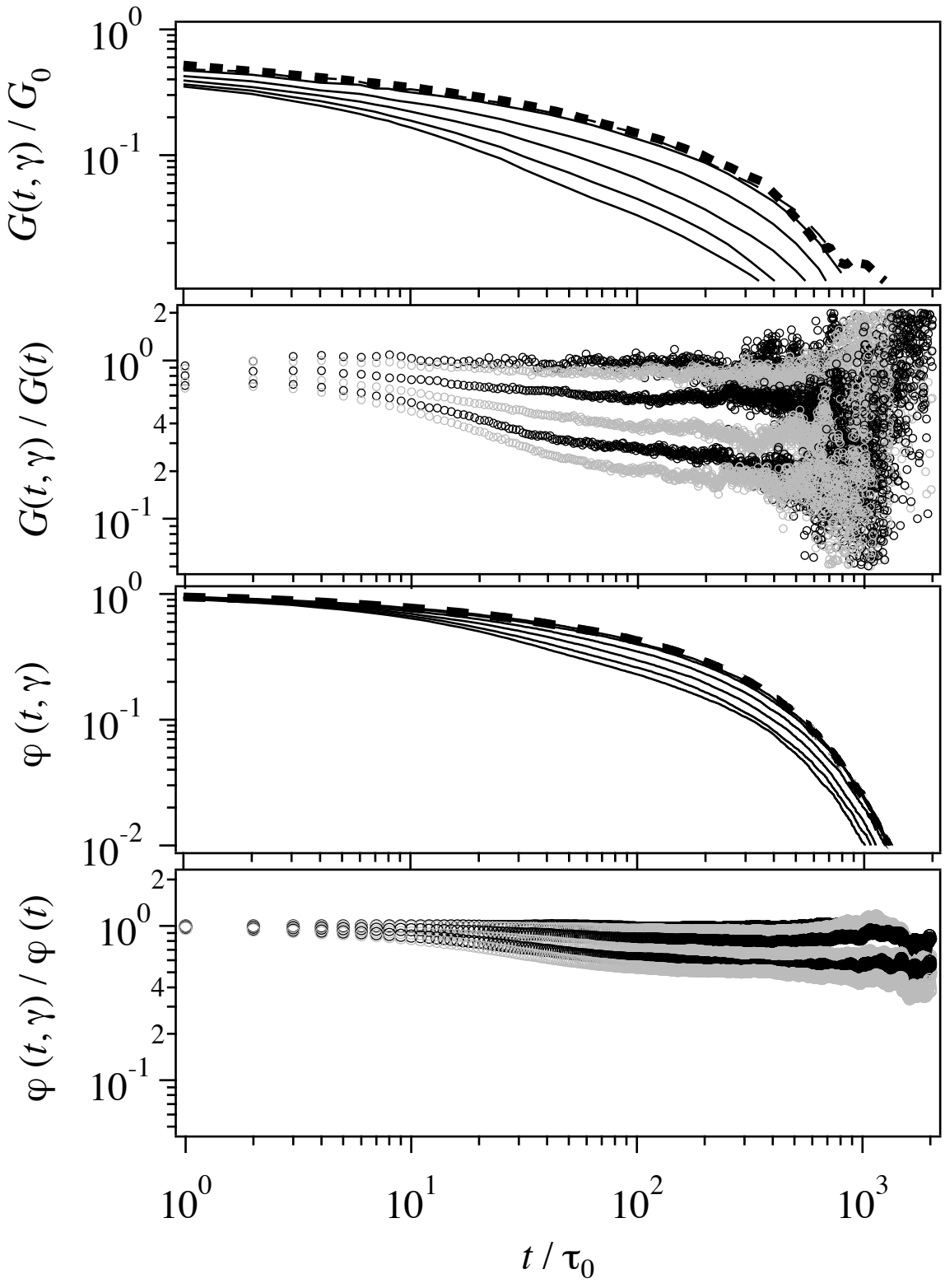

Figure 5 Masubuchi et al

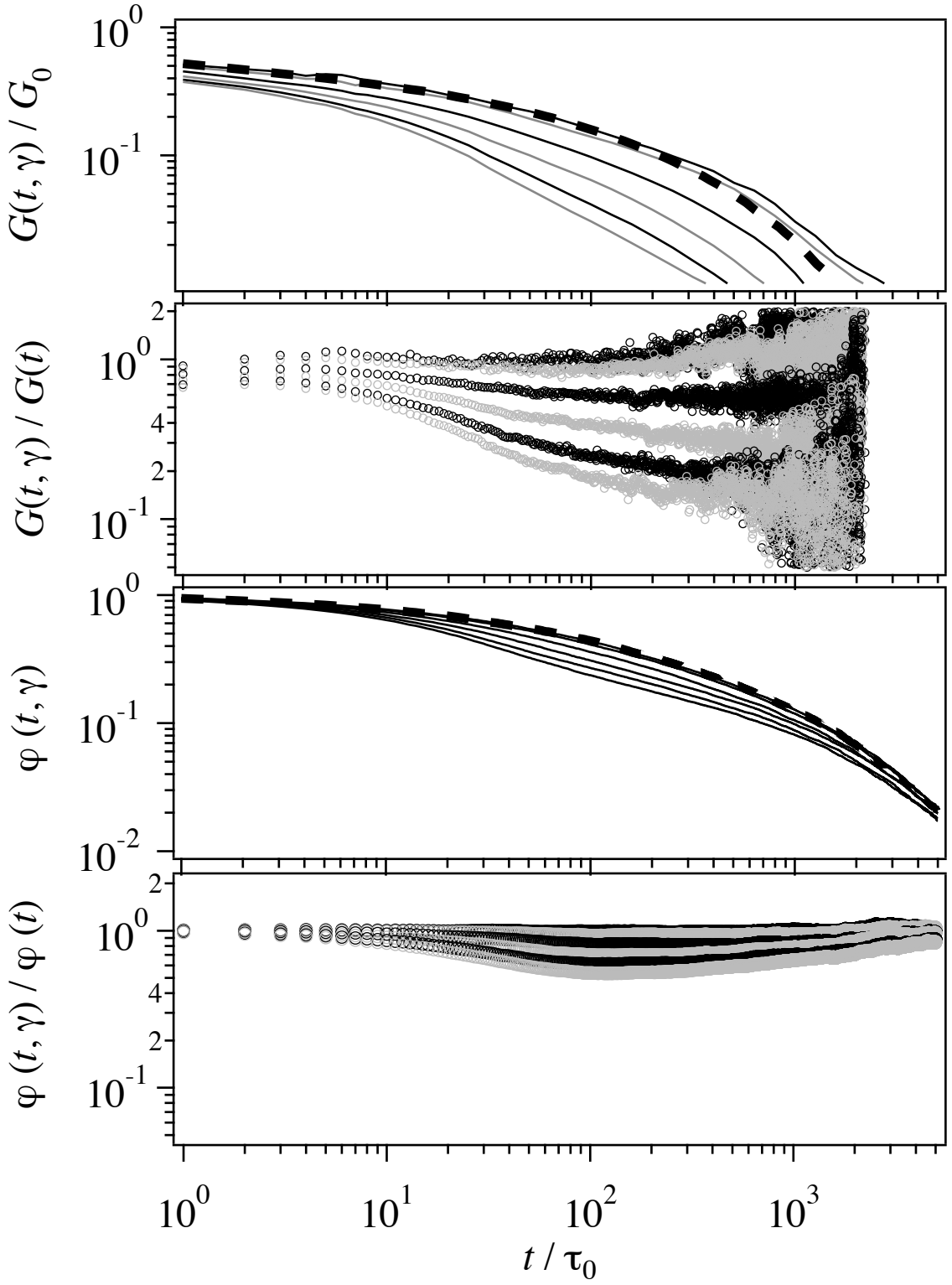

Figure 6 Masubuchi et al

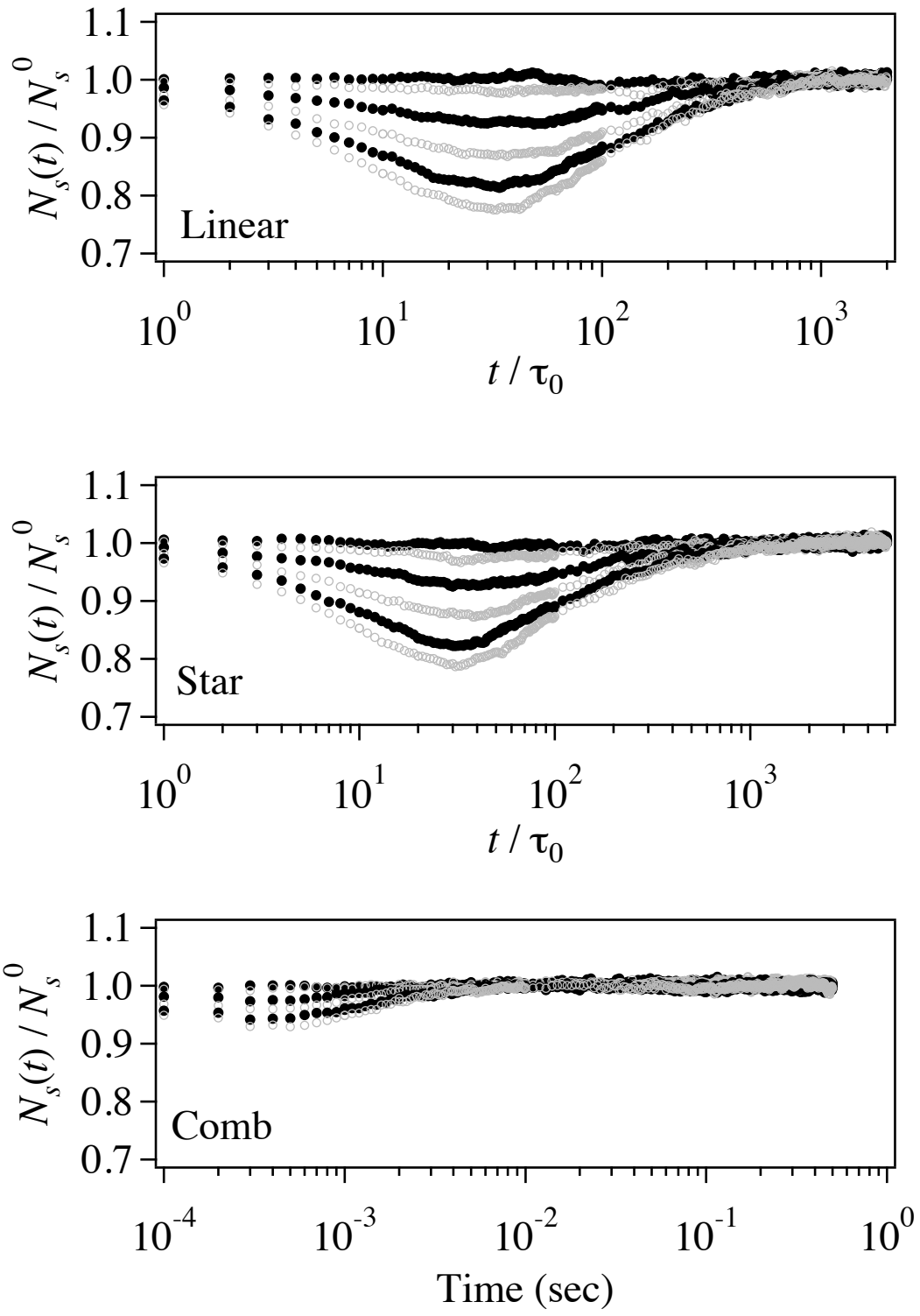

Figure 7 Masubuchi et al